Proceedings of the 10th World Congress on Mechanical, Chemical, and Material Engineering (MCM'24)
Barcelona, Spain - August 22-24, 2024
Paper No. ICMIE 127
DOI: 10.11159/icmie24.127

A Static Analysis of Compression and Torsion of Kresling Origami Springs

Kevin Kuriakose Joseph[1], Ahmed S. Dalaq[2], Mohammed F. Daqaq[3]
[1]University of Toronto, Toronto, Canada
kevink.joseph@mail.utoronto.ca
[2]King Fahd University of Petroleum and Minerals, Dammam, Saudi Arabia
ahmed.dalaq@kfupm.edu.sa
[3]New York University Abu Dhabi, Abu Dhabi, United Arab Emirates
mohammed.daqaq@nyu.edu

Abstract **-** Origami-inspired structures have increasingly been used to design various functional systems from solar cells to fluidic muscles due to their unique properties such as modulation of stiffness, and the extent of compressibility. Recently, Kresling origami springs (KOS) have gained large attention because they are deployed from compact cylindrical bellow-like structures while being able to exhibit several distinct restoring behaviours together with having a unique tension-torsion coupling. There have been few studies exploring the uni-axial response of KOS, but not the torsional aspect of the springs. In this short manuscript, we discuss the torsional response of KOS in terms of torque, relative rotation, torsional stiffness and their relation with the uni-axial response. We used a simple shell-based finite element model, specifically for KOS with a linear response (i.e. linear spring). The torsional behaviour of the KOS shown here along with the ease of manufacturing, cheap materials, and light and modular properties make origami-inspired systems a great fit for applications such as the design of torsional actuators.

Keywords**:** Non-linear Dynamics, Kresling Origami Springs, Restoring Force, Restoring Torque, Torsional Stiffness

1. Introduction

Metamaterials have unlocked and combined unusual mechanical and general physical properties. Under the umbrella of metamaterials, is the field of architected materials, where the geometric features of the material are designed for specific sets of mechanical properties [1]. The effect of geometric manipulation may also extend beyond mechanical properties to achieve unique acoustics, electromagnetic, optical, or transport properties.

Extensive studies in the field of metamaterials together with the advent of 3D printing, served in expanding the field of architected materials. By carefully designing geometric crease or fold patterns on structures and fabricating them using 3D printing, researchers are able to create 'programmed structures' through elastic energy [2]. The fold-crease patterns and design allow the structure to be 'programmed' in different configurations inducing local deformations that are independent of basic constituent (i.e. base material) or loading rate [2] [3]. Repeated patterns of origami-inspired folds and creases in structures enable the formation of various mechanical behaviours and localized configurations which are scalable. Moreover, the origami-inspired structures allow researchers to customize the mechanical stiffness and their locking behaviour [4]. Some other applications of origami structures include: rarefaction solitary wave [5], truss structures [6], and energy absorption [7].

There are two major categories among origami-inspired structures: rigid and non-rigid. Rigid origami structures are composed of rigid panels and facets which are transformable. Miura-Ori fold patterns are examples of rigid origami structures that modulate stiffness, rigidity, compressibility, and negative Poisson's ratio [8] [9]. These structures are employed in solar cells [10], electronics [11] and most recently in space applications [12] [13], most notably of which, for the deployment of James Webb Telescope [14]. Particularly, the James-Webb telescope's primary mirror comprises 18 hexagonal-shaped segments based on a rigid origami pattern, which allows for ease of deployment in space. James Webb telescope therefore has an almost 6.25 times larger collecting area than the Hubble telescope [15].

Non-rigid origami structures demonstrate elastic deformation of the panels and the creases between their facets (refer Figure 1) [16]. Recently, there have been extensive studies on the mechanics of Kresling springs, which has contributed to the development of antenna [17], fluidic muscles [18], and mechanical bit memory switches [19].

In practice, Kresling prototypes are typically made by dividing a thin paper sheet into triangles tracing the Kresling pattern and folding the paper along its edges to form valley and mountain folds. The KOS is made of similar triangles arranged in cyclic symmetry and connected together such that they form a cylindrical bellow-type structure [16] [20]. Aside from paper-based prototypes, a more functional form of Kresling springs can be formed of two-phase materials [16] [20], where rigid polymers form the relatively rigid facets and compliant rubbery material which forms the creases. Those flexible rubbery sections are characterized by thickness t. Accordingly, the entire Kresling springs design is characterized by three geometric parameters: $(\phi_o, u_o/R, w/t, N)$ as shown in Figure 1, where ϕ_o is the relative rotation angle, u_o/R is the normalized rotation height, w/t the normalized width of the flexible crease section, t is the panel thickness, R is the circumscribing radius and N is the number of sides. In this paper, we limit our analysis to a hexagonal frontal section (i.e. $N = 6$).

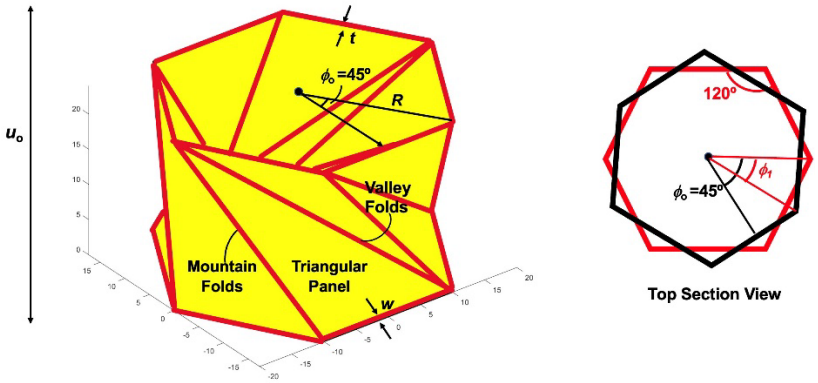

Figure 1: A Kresling Origami Spring

Qualitatively, displacing either end of the Kresling springs results in uni-axial translation combined with axial rotation. Both ends develop uni-axial force and torque as resistance to rotation and translation respectively [16] [20]. It is the rotational and the concomitant torque which is yet to be modelled and tracked during the deformation of Kresling springs. Therefore, the authors of this paper developed a simple shell-based finite element model to track the torsional resistance during deformation which will be discussed in the upcoming sections. From our previous works (Figure 2), we have found that Kresling springs is capable of exhibiting several mechanical behaviours: linear and nonlinear responses, quasi-zero stiffness (QZS) and bi-stable responses [16] [20] [21]. This study mainly investigates Kresling springs with a rotation angle of $\phi_o = 90^o$ and maps out the stiffness values of Kresling springs across from $\phi_o = 20^o$ to $\phi_o = 90^o$ (refer Figure 2).

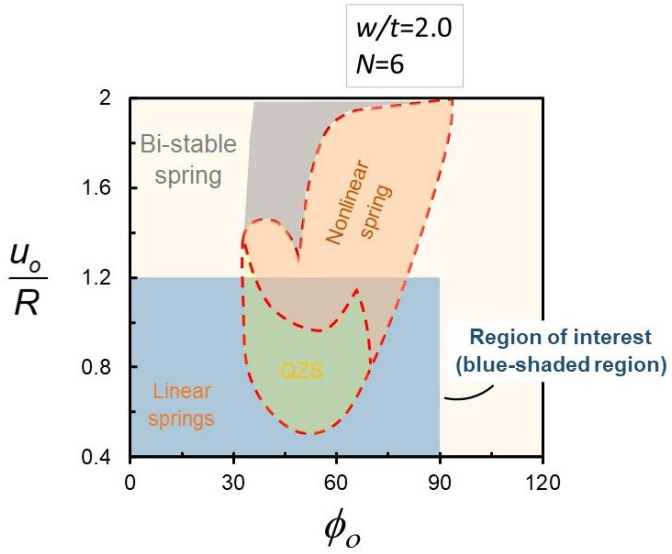

Figure 2: Region of Interest in the design map adapted from [16]

2. Methods

2.1 Generation of Origami CAD file

We used an in-house MATLAB code to automatically generate CAD files of Kresling spring models based on the desired set of geometric parameters: $(\phi_o, u_o/R, w/t, N)$. We fixed the thickness of the flexible creases flexible crease sections of $(w/t = 2)$.

2.2 Finite element modelling of Kresling Spring

Shell-based Finite Element model is prepared to simulate the mechanical response of the Kresling spring under uni-axial compression and torsion. The geometry was meshed using 4-node linear shell elements. The Kresling spring as mentioned earlier, is partitioned into two domains namely the rigid Vero indicated in yellow and the rubbery TangoBlackPlus indicated in red (refer Figure 1). Both domains are modelled with linear elastic constitutive laws with assigned Young's modulus E and Poisson's ratio ν. The parameters were fixed throughout the model, where the first domain made from flexible material TangoBlackPlus is assigned $E = 3 \times 10^5$ Pa and $\nu = 0.3$, and the second domain assigned to the rigid material (Vero) having $E = 3 \times 10^9$ Pa and $\nu = 0.3$. The parameter values for the domains are set based on actual material properties used in the fabrication of Kresling spring [20]. The thickness and radius of the panel in the Kresling spring were set as: $t = 1$ mm and $R = 20$ mm.

Two distinct sets of boundary conditions were use to analyze KOS under torsion (Figure 3a) and compression (Figure 3a). The first boundary condition at the base keeps one side of the origami spring fixed. Another set of boundary conditions applied at the top surface imposes either uni-axial displacement or rotation. The computational model outputs the restoring force F and torque T during deformation; u and ϕ.

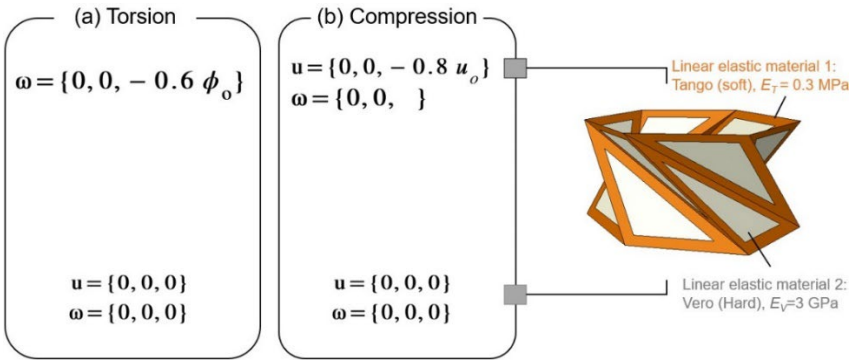

Figure 3: Applied Boundary Condition to study KOS under (a) Rotation and (b) uni-axial compression

Figure 4a shows the restoring force of Kresling spring when subjected to uni-axial quasi-static compression. The restoring force was generated to equilibrate the compression applied. The uniaxial compression results in rotation of the top surface, which is unconstrained and is free to rotate. For varied height; u_0/R from 0.4 to 1.2, the spring exhibits an almost linear trend between $\frac{F}{E_T R^2}$ (normalized reaction force) and deflection u/u_o. Non-linearity is attributed to geometric large deformations, particularly at the creases. The slope of $\frac{F}{E_T R^2} - u/u_o$ estimates the uni-axial compressive stiffness for every simulated cases, $K_c(u_o/R, \phi_o = 90^o)$ as depicted on Figure 4b.

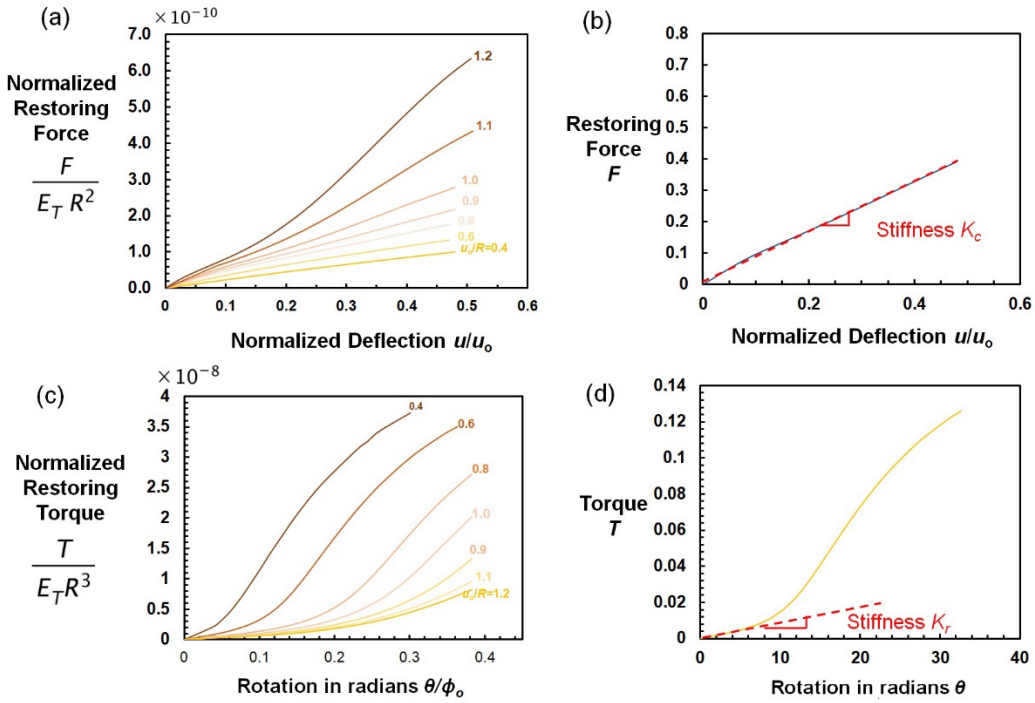

Figure 4: Quantitative Graphs from a computational model (a)Normalized Restoring Force and Deflection (b)Stiffness graph for Restoring Force and Deflection (c) Normalized Restoring Torque and Rotation (d) Stiffness graph for Restoring Torque and Rotation

3. Results and Discussion

Figure 4c shows the restoring torque T, normalized by the $E_T R^3$ as a function of the prescribed angular rotation θ/ϕ_o for various origami of height u_o. Generally for cases ranging between $\frac{uo}{R} = 0.4 - 1.2$, the restoring torque increases for a brief rotation, after which the curve shows an inflection during which the curve slope rises (i.e. hardens) by $\approx\times 10$ the initial slope (Figure 3c). Markedly, taller designs with increased u_0/R, results in smaller torque that is in contrast with uni-axial compression where higher forces are observed with taller designs. We computed the torsional stiffness K_r from the tangent slope at $\theta = 0$ of $\frac{T}{E_T R^3} - \frac{\theta}{\phi_o}$ for each design; $K_r(u_o/R, \phi_o = 90^o)$ (see Figure 4d).

3.1. Uniaxial Compression and Rotation Stiffness for Kresling spring $\phi_o = 90^o$

Both K_c and K_r are plotted in Figure 5 with increased origami height u_o/R along with their corresponding contour plot undergoing uni-axial compression and rotation respectively. Interestingly, the compressive stiffness K_c appears to be insensitive to increase in u_o/R up until $u_0/R = 0.9$. After which the K_c increases exponentially with height. As u_o/R increases, the panels become increasingly elongated, amplifying the vertical component of the forces along the uniaxial direction, which explains the rapid increase in stiffness. In contrast, the opposite is displayed during prescribed rotation. The rotational stiffness K_r starts off maximum for short cases (low u_o/R) and gradually declines with increased u_o/R. Although intuitively one may expect both stiffnesses to go hand in hand. However, this disparity between both stiffnesses is because both prescribed loadings (uni-axial displacement vs. rotation) follow two distinct loading paths of lowest potential energy [19] [21]. In simpler terms, while rotation and uniaxial compression seem to have similar qualitative kinematic effects on the Kresling springs, the forces experienced during these processes are quite distinct.

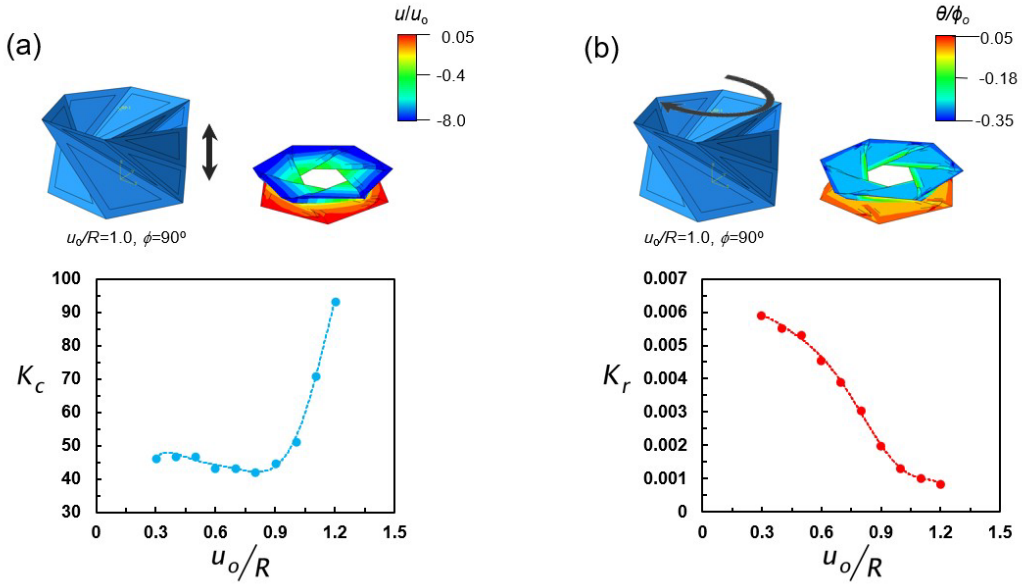

Figure 5: Field Contours (KOS $\phi_o = 90°$)

3.2 Kresling Spring Stiffness across the design space

We further analyzed the stiffness, K_c, and K_r, from simulations and present their contour plots in Figure 6 for $u_o/R = [0.3,1]$ and $\phi_o = [20°, 90°]$ under uniaxial compression and rotation (recall Figure 3). Selected Kresling springs are marked across the contour map and depicted in Figure 6a.

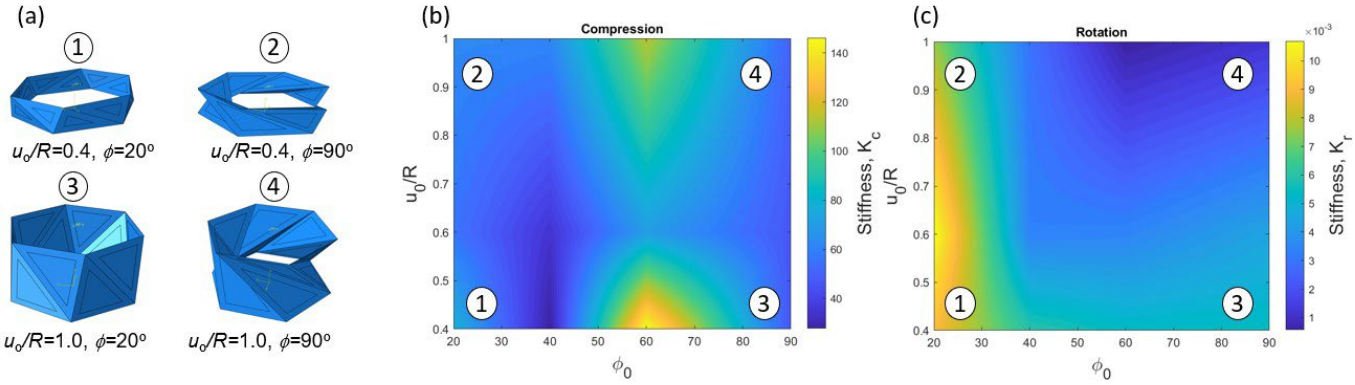

Figure 6: Field Contours across design space

The compressive stiffness of the Kresling spring is lowest at ϕ_o but peaks at $\phi_o = 60°$, declining rapidly thereafter. The lowest K_c values are registered for shorter springs, typically around $\phi_o = 40°$. Increased height stiffens the spring's K_c.

Maximum rotational stiffness is achieved in designs with the lowest relative angle ϕ_o. Increasing both ϕ_o and u_o/R, moving diagonally across the design space, reduces K_r. The lowest K_r values occur around $u_o/R = 1$ and $\phi_o = 60°$, which is the complete opposite of compressive stiffness, whereat, peak K_r occurs. Increased height generally decreases rotational stiffness, while changes in the relative angle have a negligible influence on K_r.

4. Conclusion

In this paper, we utilized a shell-based finite element model to predict the behavior of cylindrical Kresling springs under torsion and uniaxial compression. Our study focused on 6-sided Kresling Origami Structures (KOS) with a linear elastic constitutive law for the constituent materials. Although these materials exhibit linear elastic responses under uniaxial compression, the resulting torque exhibits a linear response initially but eventually displays non-linearity at later stages during rotation.

Increasing the height of the spring leads to a stiffer uniaxial response but, surprisingly, results in a softer response in torsion. In other words, taller springs are easier to rotate but harder to compress. This unique difference in stiffness can selectively trigger or actuate the Kresling spring through torsion, effectively filtering out compressive loads to allow rotational activation of the system. Conversely, for shorter Kresling spring designs, compression activates the system instead of torsion.

Finally, structures and materials with variable torsional stiffness values hold significant importance in the field of robotics [22] [23], and these origami configurations can be further exploited for applications, including programmable actuators [24].

References

[1] L. T. Govindaraman, A. Arjunan, A. Baroutaji, J. Robinson and A.-G. Olabi, "Metamaterials for Energy Harvesting," in *Encyclopedia of Smart Materials*, A. Olabi, Ed., Oxford, Elsevier, 2022, p. 522–534.

[2] S. Shan, S. H. Kang, J. R. Raney, P. Wang, L. Fang, F. Candido, J. A. Lewis and K. Bertoldi, "Multistable Architected Materials for Trapping Elastic Strain Energy," *Advanced Materials,* vol. 27, p. 4296–4301, 2015.

[3] S. Li, H. Fang, S. Sadeghi, P. Bhovad and K.-W. Wang, "Architected Origami Materials: How Folding Creates Sophisticated Mechanical Properties," *Advanced Materials,* vol. 31, p. 1805282, 2019.

[4] Y. Miyazawa, H. Yasuda, H. Kim, J. H. Lynch, K. Tsujikawa, T. Kunimine, J. R. Raney and J. Yang, "Heterogeneous origami-architected materials with variable stiffness," *Communications Materials,* vol. 2, p. 1–7, November 2021.

[5] H. Yasuda, Y. Miyazawa, E. G. Charalampidis, C. Chong, P. G. Kevrekidis and J. Yang, "Origami-based impact mitigation via rarefaction solitary wave creation," *Science Advances,* vol. 5, p. eaau2835, May 2019.

[6] H. Yasuda, T. Tachi, M. Lee and J. Yang, "Origami-based tunable truss structures for non-volatile mechanical memory operation," *Nature Communications,* vol. 8, 2017.

[7] Z. Chen, T. Wu, G. Nian, Y. Shan, X. Liang, H. Jiang and S. Qu, "Ron Resch Origami Pattern Inspired Energy Absorption Structures," *Journal of Applied Mechanics,* vol. 86, October 2018.

[8] N. Kidambi and K. W. Wang, "Dynamics of Kresling origami deployment," *Physical Review E,* vol. 101, p. 063003, June 2020.

[9] T. Tachi, "Geometric Considerations for the Design of Rigid Origami Structures," *Proceedings of the International Association for Shell and Spatial Structures (IASS) Symposium,* January 2010.

[10] R. Tang, H. Huang, H. Tu, H. Liang, M. Liang, Z. Song, Y. Xu, H. Jiang and H. Yu, "Origami-enabled deformable silicon solar cells," *Applied Physics Letters,* vol. 104, p. 083501, February 2014.

[11] Z. Song, T. Ma, R. Tang, Q. Cheng, X. Wang, D. Krishnaraju, R. Panat, C. K. Chan, H. Yu and H. Jiang, "Origami lithium-ion batteries," *Nature Communications,* vol. 5, 2014.

[12] Y. Nishiyama, "Miura folding: Applying origami to space exploration," *International Journal of Pure and Applied Mathematics,* vol. 79, p. 269–279, 2012.

[13] K. Miura, "Method of Packaging and Deployment of Large Membranes in Space," *The Institute of Space and Astronautical Science report,* vol. 618, p. 1–9, March 2015.

[14] R. Irion, "Origami Observatory," *Scientific American,* vol. 303, p. 48–55, 2010.

[15] J. C. Mather, "The James Webb Space Telescope Mission," *AIP Conference Proceedings,* vol. 1294, p. 1–8, November 2010.

[16] A. S. Dalaq and M. F. Daqaq, "Experimentally-validated computational modeling and characterization of the quasi-static behavior of functional 3D-printed origami-inspired springs," *Materials & Design,* vol. 216, p. 110541, April 2022.

[17] S. Yao, X. Liu, S. V. Georgakopoulos and M. M. Tentzeris, "A novel tunable origami accordion antenna," in *2014 IEEE Antennas and Propagation Society International Symposium (APSURSI)*, 2014.

[18] S. Li, D. M. Vogt, D. Rus and R. J. Wood, "Fluid-driven origami-inspired artificial muscles," *Proceedings of the National Academy of Sciences,* vol. 114, p. 13132–13137, December 2017.

[19] R. Masana, S. Khazaaleh, H. Alhussein, R. S. Crespo and M. F. Daqaq, "An origami-inspired dynamically actuated binary switch," *Applied Physics Letters,* vol. 117, p. 081901, August 2020.

[20] S. Khazaaleh, R. Masana and M. F. Daqaq, "Functional, Durable, and Scalable Origami-Inspired Springs," *Composites Part B: Engineering,* vol. 236, p. 109811, May 2022.

[21] R. Masana and M. F. Daqaq, "Equilibria and bifurcations of a foldable paper-based spring inspired by Kresling-pattern origami," *Phys. Rev. E,* vol. 100, no. 6, p. 063001, December 2019.

[22] J. Santoso, E. H. Skorina, M. Luo, R. Yan and C. D. Onal, "Design and analysis of an origami continuum manipulation module with torsional strength," in *2017 IEEE/RSJ International Conference on Intelligent Robots and Systems (IROS)*, 2017.

[23] J. Santoso and C. D. Onal, "An Origami Continuum Robot Capable of Precise Motion Through Torsionally Stiff Body and Smooth Inverse Kinematics," *Soft Robotics,* vol. 8, p. 371–386, August 2021.

[24] D. Tang, C. Zhang, H. Sun, H. Dai, J. Xie, J. Fu and P. Zhao, "Origami-inspired magnetic-driven soft actuators with programmable designs and multiple applications," *Nano Energy,* vol. 89, p. 106424, November 2021.